Acta Cryst. (1999). B**55**, 853–866

Symmetry classification of the layered perovskite-derived $A_nB_nX_{3n+2}$ structures

Igor Levin* and Leonid A. Bendersky

National Institute of Standards and Technology, Materials Science and Engineering Laboratory, Gaithersburg, MD 20899, USA. E-mail: igorl@mailserver.nist.gov

(*Received 13 October 1998; accepted 19 April 1999*)

Abstract

The effects of combinations of octahedral tilts on the symmetries of layered $A_nB_nX_{3n+2}$ structures were considered. Two complementary approaches were used to deduce the symmetries. The space groups associated with different tilt systems were determined for structures with different layer thicknesses (n values) and for structures with different layer stacking arrangements. For the most symmetrical tilts about the orthorhombic axes of the $A_nB_nX_{3n+2}$ structure, maximal group/subgroup relations were established. Comparison of these results with experimental data available in the literature suggests that the symmetries of most observed $A_nB_nX_{3n+2}$ compounds are fully determined by the tilt systems adopted by rigid BX_6 octahedra. The most common tilt system observed at room temperature is a combination of an in-phase tilt about an orthorhombic axis parallel to the pseudo-fourfold axis of the octahedron with a tilt about an orthorhombic axis perpendicular to the layers.

1. Introduction

Many compounds crystallize in structures composed of layers (slabs) of the perovskite-type structure, ABX_3, in which BX_6 octahedra share all corners. These structures can be classified according to the layer-orientation relative to the principle axes of an ideal cubic perovskite structure. Three major groups of such compounds, with the layer plane parallel to either $\{001\}_c$, $\{110\}_c$ or $\{111\}_c$ (c = cubic), have been identified and described as the structural series $A_{n+1}B_nX_{3n+1}$, $A_nB_nX_{3n+2}$ and $A_{n+1}B_nX_{3n+3}$, respectively (Wells, 1984; Weiden *et al.*, 1995). In these formulae, n represents the number of BX_6 octahedra that span a layer, and therefore specifies the layer thickness. In structures in which layers of different thicknesses are mixed, n is non-integral and indicates the average number of octahedra per layer.

Many of the $A_{n+1}B_nX_{3n+1}$ compounds (Ruddlesden–Popper phases) exhibit high-temperature superconductivity, and therefore have been studied intensively. The $A_nB_nX_{3n+2}$ phases also have interesting properties. For example, many of the fully oxidized compounds are ferroelectrics with high Curie temperatures, and in some, ferroelectricity is combined with excellent piezoelectric and electrooptic properties (Nanamatsu & Kimura, 1974; Nanamatsu *et al.*, 1974). Reduction of certain $A_nB_nX_{3n+2}$ compounds (B = Ti, Nb; n = 4) has resulted in semiconducting behavior between room temperature and 4 K (Schmalle *et al.*, 1995). The possibility of coexisting insulator–conductor behavior in partially reduced $A_nB_nX_{3n+2}$ compounds with mixed layers has also been proposed (Bednorz, 1997). Detailed crystallographic analysis of this system is needed to elucidate structural details that could be related to the observed properties.

Members of the $A_nB_nX_{3n+2}$ structural series, with $2 \leq n \leq 7$, have been identified in a number of inorganic systems, predominately with X = O and F. The results of our literature survey on these compounds are summarized in Table 1. The number of observed compounds decreases as the n value increases, and compounds with non-integer n values are relatively rare. Analysis of the crystallographic data shows that: (*a*) $A_nB_nX_{3n+2}$ structures crystallize in a variety of space groups, all of which are either orthorhombic or monoclinic; (*b*) compounds with the same n value, but different symmetries, correspond to different distortions of the layers relative to the ideal cubic perovskite structure; (*c*) in several compounds (*e.g.* $BaMnF_4$, $La_2Ti_2O_7$, $Sr_2Nb_2O_7$) reversible polymorphic phase transitions have been associated with changes in octahedral tilt systems. Some compounds were reported to be incommensurate at low temperatures, and the modulation waves were attributed to octahedral tilting (Sciau *et al.*, 1988; Yamamoto, 1982; Nanot *et al.*, 1981).

In many three-dimensional perovskite-like structures, the symmetry reduction relative to ideal cubic ($Pm\bar{3}m$) is determined entirely by tilting of rigid octahedra (Megaw, 1973; Woodward, 1997*a*). A classification scheme which relates all the possible (23) tilt systems (combination of tilts about fourfold axes of the octahedron) to the space groups of the resulting distorted structures was originally proposed by Glazer (1972) and subsequently confirmed by Alexandrov (1976) and Woodward (1997*a*,*b*). The crystallographic analysis developed by Glazer for the three-dimensional perovskite-like structures was extended to treat the layered ABX_4 and A_2BX_4 compounds (Deblieck *et al.*, 1985;

Table 1. *Summary of the experimental data on $A_nB_nX_{3n+2}$ type structures*

Tilt system approximating the structural distortion was assigned only to the structures with atomic positions refined. IC refers to the incommensurate structure. Some compounds were reported in the literature in Russian only. For these compounds the reference is given to the book by Alexandrov & Beznosikov (1997).

Phase	n	Space group at room temperature	Tilt system	Reference
$BaMgF_4$	2	$Cmc2_1$	$\mathbf{a}^+$	Keve *et al.* (1969, 1970), Di Domenico *et al.* (1969)
$BaFeF_4$	2	$Cmc2_1$	$\mathbf{a}^+$	Keve *et al.* (1969, 1970)
$BaMnF_4$	2	IC	$\mathbf{a}^+\mathbf{c}$	Sciau *et al.* (1988)
$BaCoF_4$	2	$Cmc2_1$	$\mathbf{a}^+$	Keve *et al.* (1969), Schnering & Bleckman (1968)
$BaZnF_4$	2	$Cmc2_1$	$\mathbf{a}^+$	Keve *et al.* (1969), Schnering & Bleckman (1968)
$BaCuF_4$		$Cmc2_1$	$\mathbf{a}^+$	Dance (1981)
$NaCrF_4$	2	$P112_1/a$	$\mathbf{a}^-\mathbf{b}$	Knoke *et al.* (1979)
$Ba_2Zn_2F_7Cl$	2	$P112_1/m$	$\mathbf{c}$	Maguer *et al.* (1995)
$Ba_2Co_2F_7Cl$	2	$P112_1/m$	$\mathbf{c}$	Maguer *et al.* (1995)
$Sr_2Nb_2O_7$	4	$Cmc2_1$	$\mathbf{a}^+$	Ishizawa *et al.* (1975)
		$Pbn2_1$	$\mathbf{a}^+\mathbf{b}$	Scheunemann & Müller-Buschbaum (1975*a*)
		IC	$\mathbf{a}^+\mathbf{b}$	Yamamoto *et al.* (1980)
$SrLaTiNbO_7$	4	*o*	–	Alexandrov & Beznosikov (1997)
$SrLaTiTaO_7$	4	*o*	–	Alexandrov & Beznosikov (1997)
$SrNdTiTaO_7$	4	$Pbn2_1$	$\mathbf{a}^+\mathbf{b}$	Alexandrov & Beznosikov (1997)
$SrPrTiTaO_7$	4	*o*	–	Alexandrov & Beznosikov (1997)
$Sr_2Ta_2O_7$	4	*Cmcm*	–	Nanamatsu *et al.* (1975)
		$P2_1/m$	–	Yamamoto *et al.* (1980)
$Ca_2Nb_2O_7$	4	$P2_1$	$\mathbf{a}^+\mathbf{b}$	Brandon & Megaw (1970), Nanamatsu & Kimura (1974)
		$Pbn2_1$	$\mathbf{a}^+\mathbf{b}$	Scheunemann & Müller-Buschbaum (1974)
$CaLaTiNbO_7$	4	$Pbn2_1$	$\mathbf{a}^+\mathbf{b}$	Alexandrov & Beznosikov (1997)
$La_2Ti_2O_7$	4	$Pbn2_1$	$\mathbf{a}^+\mathbf{b}$	Scheunemann & Müller-Buschbaum (1975*b*)
		$P2_1$	$\mathbf{a}^+\mathbf{b}$	Gasperin (1975), Tanaka *et al.* (1985)
$La_2TiSc_{1/2}Nb_{1/2}O_7$	4	$Pbn2_1$	$\mathbf{a}^+\mathbf{b}$	Sych & Titov (1981*a*)
$La_2TiMg_{1/3}Nb_{2/3}O_7$	4	*o*	–	Sych & Titov (1981*b*)
$Pr_2Ti_2O_7$	4	$P2_1$	$\mathbf{a}^+\mathbf{b}$	Koz'Min *et al.* (1997)
Nd_2TiO_7	4	*m*	–	Williams *et al.* (1993)
$Sm_2Ti_2O_7$	4	*m*	–	Alexandrov & Beznosikov (1997)
$Ce_2Ti_2O_7$	4	$P2_1$	$\mathbf{a}^+\mathbf{b}$	Alexandrov & Beznosikov (1997)
$La_{4.33}Ti_{4.33}O_{15}$	4.33	–	-	Williams *et al.* (1993)
$La_4Ca_{0.5}Ti_{4.5}O_{15.5}$	4.5	$P112_1/b$ or $P112_1$	–	Nanot *et al.* (1979, 1986, 1981)
$Nd_4Ca_{0.5}Ti_{4.5}O_{15.5}$	4.5	$P112_1/b$ or $P112_1$	–	Nanot *et al.* (1979, 1986, 1981)
$Ca_{4.5}Nb_4Ti_{0.5}O_{15.5}$	4.5	$P112_1/b$ or $P112_1$	–	Nanot *et al.* (1979, 1986, 1981)
$Nd_4CaTi_5O_{17}$		$P112_1/b$ or $P112_1$	–	Nanot *et al.* (1979, 1986, 1981)
$Ca_5Nb_4TiO_{17}$		$P112_1/b$ or $P112_1$	–	Nanot *et al.* (1979, 1986, 1981)
$La_4CaTi_5O_{17}$		$P112_1/b$ or $P112_1$	–	Nanot *et al.* (1979, 1986, 1981)
$Sr_5Nb_5O_{17}$	5	*Pnn*2	$\mathbf{a}^+$	Schmalle *et al.* (1995)
$La_5Ti_5O_{17}$	5	–	–	Williams *et al.* (1993)
$Ca_5Nb_5O_{17}$	5	–	–	Williams *et al.* (1993)
$Sr_5TiNb_4O_{17}$	5	*Pmnn*	$\mathbf{a}^+$	Isupov *et al.* (1977), Drews *et al.* (1996)
$Sr_6Ti_2Nb_4O_{20}$	6	$Cmc2_1$	–	Isupov *et al.* (1976)
$Nd_4Ca_2Ti_6O_{20}$	6	$Pbn2_1$	–	Nanot *et al.* (1979, 1986, 1981)
$La_4Ca_2Ti_6O_{20}$	6	$P2_1$	–	Nanot *et al.* (1979, 1986, 1981)
$Ca_6Nb_4Ti_6O_{20}$	6	$P2_1$	–	Nanot *et al.* (1979, 1986, 1981)
$Sr_7Ti_3Nb_4O_{23}$	7	IC	–	Levin *et al.* (1999)

Alexandrov *et al.*, 1987; Alexandrov & Bartolomé, 1994). Group-theoretical analysis was also applied to analyze the effects of octahedral tilting on symmetry (Alexandrov *et al.*, 1987; Hatch & Stokes, 1987; Howard & Stokes, 1998). Both methods yielded identical results. Comparison of the experimentally determined space groups for various ABX_4 and A_2BX_4 compounds with those predicted by the analysis, confirms that the symmetries of distorted structures are approximated well by tilting of rigid BX_6 octahedra, with the positions of the A cations adopting the specific symmetry reduction. Group/subgroup relations between structures of maximal symmetry (aristotype) and tilted structures of lower symmetry (hettotypes), which describe possible phase-transition paths, have also been established (Deblieck *et al.*, 1985).

Despite many crystallographic studies of $A_nB_nX_{3n+2}$ compounds (Table 1), no systematic relationships between the space-group symmetries and octahedral tilting systems have been proposed. Here we present a general crystallographic analysis of the $A_nB_nX_{3n+2}$ structures; in a subsequent report (Levin *et al.*, 1999) an experimental study of a series of $Sr_n(Nb,Ti)_nX_{3n+2}$ compounds will be described. The symmetry analysis

focuses on the effects of (*a*) layer thickness, (*b*) layer mixing and (*c*) octahedral tilt system(s) on the symmetries of $A_nB_nX_{3n+2}$ structures.

2. Symmetry of $A_nB_nX_{3n+2}$ structures with untilted octahedra

In this work, we adopted the setting of axes used for the orthorhombic *Cmcm* structure of the high-temperature $Sr_2Nb_2O_7$ phase ($n = 4$), a schematic drawing of which is shown in Fig. 1. In this setting, the perovskite layers are stacked in the direction of the **b** axis ($\|\|[110]_c$), and both the **a** ($\|\|[001]_c$) and the **c** ($\|\|[1\bar{1}0]_c$) axis are parallel to the layer plane. Lattice parameters of the idealized $A_nB_nX_{3n+2}$ structure can be expressed in the units of the lattice parameter of a cubic perovskite, a_c: $a_o = a_c$, $c_o = 2^{1/2}a_c$ and $b_o = (n+1)2^{1/2}a_c$. The interlayer region, further referred to as a 'spacer', is approximately one octahedron in width, $s = (2^{1/2}/2)a_c$. Octahedra on both sides of a spacer are shifted with respect to each other by the translation vector $\mathbf{R} = 1/2\mathbf{a} + \mathbf{s} = (3^{1/2}/2)a_c$, shown in Fig. 1. For a structure composed of identical layers (n = integer), a single layer will be a *motif*, *i.e.* a distinct repeat unit. For a structure with mixed layers (n = non-integer), the motif contains several layers.

2.1. *Classification of motifs*

We classified the motifs according to the relationship between the position of octahedra on opposite faces of a motif. Two types of single-layer motifs can be distinguished: motif '**o**' with an odd number of octahedra, and motif '**e**' with an even number. For an '**o**' layer, the octahedra on both faces are in a similar '0' position, and, therefore, the '**o**' motif is designated [00] (Fig. 2*a*). The [00] motif has a mirror plane in the middle. In '**e**' layers, the octahedra are related by a shift along the **c** direction ('0' and '1' positions), and this motif is labeled as [01] (Fig. 2*b*). Opposite faces in the [01] motif are related by a *c* glide. For a 'compound motif', with arbitrary combinations of different layers, two additional types, [0$\underline{0}$] and [0$\underline{1}$], are possible, where the underlined symbols represent additional shifts along the **a** direction. Examples of the [0$\underline{0}$] and [0$\underline{1}$] motifs are shown in Figs. 2(*c*) and (*d*), where the [0$\underline{0}$] motif is a combination of '**e**' and '**o**' layers, {**eo**}, and the [0$\underline{1}$] motif is a combination of two '**o**' layers of different thickness, {**oo**′}. Examples of

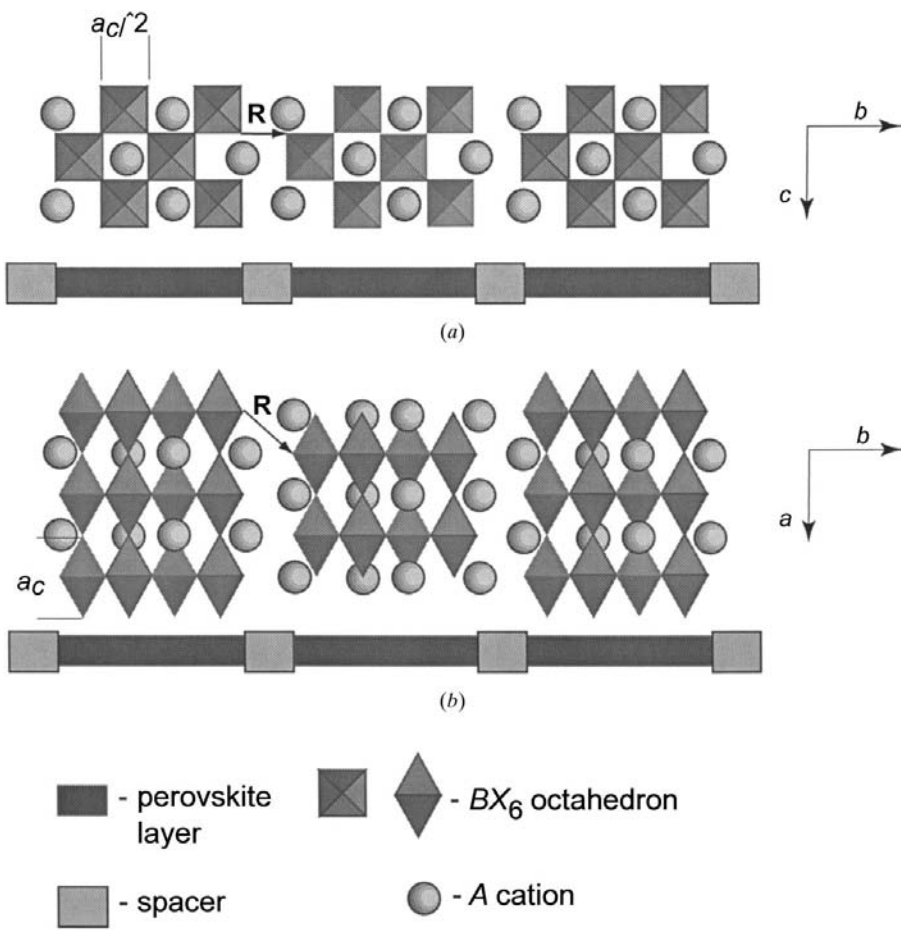

Fig. 1. Schematic projections of the orthorhombic $A_2B_2X_7$ structure along both (*a*) the [100] and (*b*) the [001] direction. The structure can be viewed as derived from the cubic perovskite structure by periodic crystallographic shears with the displacement vector **R**.

Table 2. *Classification of the motifs possible in $A_nB_nX_{3n+2}$ structures*

The Bravais lattices for the untilted structures are indicated. N_{lm} and N_{om} refer to the number of layers in a motif and the number of octahedra across a motif correspondingly.

Type of motif	N_{lm}	N_{om}	Bravais lattice, lattic parameters
[00]	$2k+1$	$2i+1$	**I**; $a = 2^{1/2}a_o$; $c = 2a_o$; $b = 2(n+1)a_o$
[01]	$2k+1$	$2i$	**C**; $a = 2^{1/2}a_o$; $c = 2a_o$; $b = 2(n+1)a_o$
[$\underline{00}$]	$2k$	$2i+1$	**A**; $a = 2^{1/2}a_o$; $c = 2a_o$; $b = 2(n+1)a_o$
[$\underline{01}$]	$2k$	$2i$	**P**; $a = 2^{1/2}a_o$; $c = 2a_o$; $b = (n+1)a_o$

the compound [00] and [01] motifs are **{oee}** and **{oeo}**, respectively. Generally, the type of motif is determined by the number of layers in a motif, N_{lm}, and the total number of octahedra that span the motif, N_{om}. The possible combinations of even and odd numbers (N_{lm}, N_{om}) represent four types of motif, as summarized in column one of Table 2.

2.2. *Bravais lattices of the untilted structures*

Translation of the [00], [01] and [$\underline{00}$] motifs (across the spacer) in the **b** direction results in the **I**-, **C**- and **A**-centered Bravais lattices, respectively. For the [$\underline{01}$] motif the lattice is primitive **P**. All four lattices have identical **a** and **c** parameters (equal two-dimensional periodicity of the layers; Table 2).

2.3. *Space groups of the untilted structures*

In structures with untilted octahedra, symmetry planes of a motif that are perpendicular to the layer plane are not removed by a translation and remain as elements of the space group. Symmetry differences

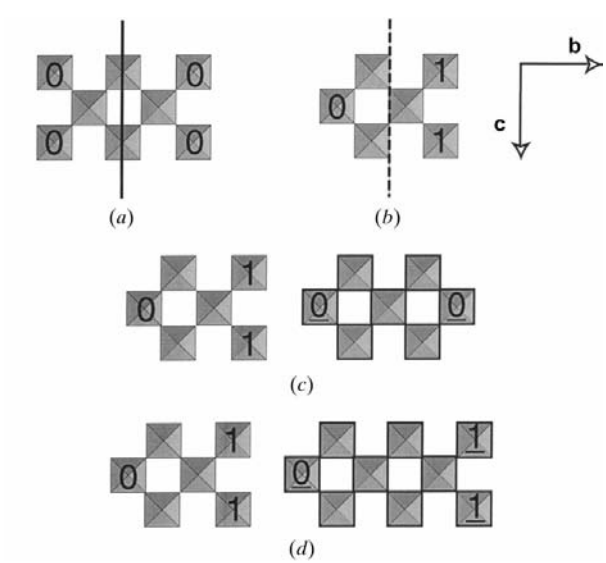

Fig. 2. Four possible type of motifs: (*a*) [00], (*b*) [01], (*c*) [$\underline{00}$] and (*d*) [$\underline{01}$].

Table 3. *Space groups for the untilted structures composed of all possible types of motifs*

Type of motif; N_{lm}/N_{om}	Lattice	Stacking sequences	Space group (standard setting)
[00]; $(2k+1)/(2i+1)$	**I**	{**o**}, {**oee**}	*Immm*
		{**oe′e**}	*Im2m* (= *Imm*2)
[01]; $(2k+1)/(2i)$	**C**	{**e**}, {**eoo**}	*Cmcm*
		{**eo′o**}	*Cm2m* (= *Amm*2)
[$\underline{00}$]; $(2k)/(2i+1)$	**A**	{**eo**}, {**oeee**}, {**oooe**}	*Ammm* (= *Cmmm*)
		{**oee′e′**}	*Am2m* (= *Amm*2)
[$\underline{01}$]; $(2k)/(2i)$	**P**	{**ee′**}	*Pmcm* (= *Pmma*)
		{**oo′**}	*Pmmm*
		{**oeeo**}	*Pmnm* (= *Pmmn*)
		{**ee′oo**}	*Pm2m* (= *Pmm*2)

between various untilted structures are primarily determined by the distribution of symmetry planes which are parallel to the layers (**b** direction). The presence of these planes depends on the particular combination of layers in a motif and is easily deduced by representing the stacking sequence as a row of the '**e**' and '**o**' letters. Following this approach, the space groups of structures with all the possible stacking sequences were derived. Our analysis shows that all the $A_nB_nX_{3n+2}$ untilted structures are represented by only ten distinct space groups (Table 3).

3. Effect of octahedral tilting on the symmetry of $A_nB_nX_{3n+2}$ structures

In the previous section, the symmetries of all untilted $A_nB_nO_{3n+2}$ structures were determined for all possible sequences of the layers. Such a general symmetry analysis for the structures with octahedral tilting is much more complicated and probably impractical. The analysis was therefore restricted to those structures in which layers of a similar type (**e** or **o**) have equal thickness. For such structures there are only four types of motif (see Table 3; {**e**}, {**o**}, {**eo**} and {**eooe**}, rather than {**ee′**}). Some further restrictions on the sense of octahedral tilts in different layers were also introduced.

3.1. *Tilt systems of a single {110} layer*

In the analysis of perovskite structures with tilted octahedra (Glazer, 1972; Alexandrov, 1976), an arbitrary tilt of an octahedron has been described by a combination of rotations about its three fourfold axes (Fig. 3*a*). This analysis assumes that for small tilts ($< 10^\circ$) the resulting structure does not depend on a tilt sequence. Both corner-sharing connectivity and rigidity of octahedra impose an alternation of the sign (phase) of tilting for the octahedra laying in a plane *normal* to the rotation axis. Tilting of successive octahedra *along* the rotation axis is unconstrained, and therefore can be

either in-phase (+) or anti-phase (−). In Glazer's notation scheme, widely accepted in the literature, any tilt system is described by a combination of three letters (**a**, **b** and **c**), which specify the tilt axis and the corresponding degree of rotation. The superscript of the letter indicates a phase relation for the rotation along the corresponding axis. For example, the symbol $\mathbf{a}^+\mathbf{a}^0\mathbf{a}^0$ describes a single in-phase tilt about the *x* axis (0 = zero rotation), while $\mathbf{a}^-\mathbf{b}^-\mathbf{c}^+$ corresponds to the anti-phase tilts about both the *x* and *y* axis, and the in-phase tilt about the third axis *z*. In the $\mathbf{a}^-\mathbf{b}^-\mathbf{c}^+$ tilt system, the magnitudes of the tilts about each of the axes are different.

In the ideal perovskite structure, all three fourfold tilt axes are equivalent, and therefore any permutation of the letters in a Glazer's symbol describes the same structure (*e.g.* $\mathbf{a}^+\mathbf{a}^0\mathbf{a}^0 = \mathbf{a}^0\mathbf{a}^0\mathbf{a}^+$). For the $\{110\}_c$ layer, the fourfold axis lying in a layer plane (parallel to the orthorhombic **a** axis) is not equivalent to the two other out-of-plane fourfold axes (Fig. 3*b*). Thus, permutation of letters in a Glazer's symbol results in the tilt symbols that correspond to different structures. For example, a single tilt system $\mathbf{a}^+\mathbf{a}^0\mathbf{a}^0$ of perovskite splits into two different tilt systems of a layer, $\mathbf{a}^+\mathbf{a}^0\mathbf{a}^0$ and $\mathbf{a}^0\mathbf{a}^0\mathbf{a}^+$. In some cases, two different Glazer's tilt systems correspond to a single tilt system of a layer: *e.g.* $\mathbf{a}^-\mathbf{b}^-\mathbf{b}^-$ and $\mathbf{a}^-\mathbf{a}^-\mathbf{a}^-$. Thus, 23 Glazer's tilt systems of a three-dimensional perovskite result in 27 tilt systems of {110}-type layers (*Appendix A*). To distinguish between these tilt systems, the Greek letters α, β and γ are used to index layers, where the 'α' is used for a tilt about the **a** axis (in a layer plane).

For an isolated octahedron, a sum of the tilts of equal magnitude ($0\beta\beta$) about both out-of-plane fourfold axes (x, y) is equivalent to a single tilt about one of its twofold axes, parallel to either the **b** or the **c** orthorhombic axis of the $A_nB_nX_{3n+2}$ structure (Figs. 3*c* and *d*). A particular choice of rotation axis (either **b** or **c**) determines the signs of both tilts. It is convenient to describe those tilt systems which involve rotations of *all* octahedra about the *same* orthorhombic **a**, **b** or **c** axes as **a**, **b** or **c** tilts, respectively (last column, Tables 4 and 5). Tilt systems (15 out of 27) which combine in-phase rotations about both out-of-plane fourfold axes (*e.g.* $\alpha^0\beta^+\beta^+$), or in-phase rotation about one of these axes and anti-phase rotation about another (*e.g.* $\alpha^0\beta^-\beta^+$), produce doubling of periodicity in both the **a** and the **c** direction. To our knowledge, no structures with a doubled *c* lattice parameter have yet been reported; therefore, we will limit the present discussion to the 12 tilt systems which leave the *c* lattice parameter unchanged (column 2, Tables 4 and 5).

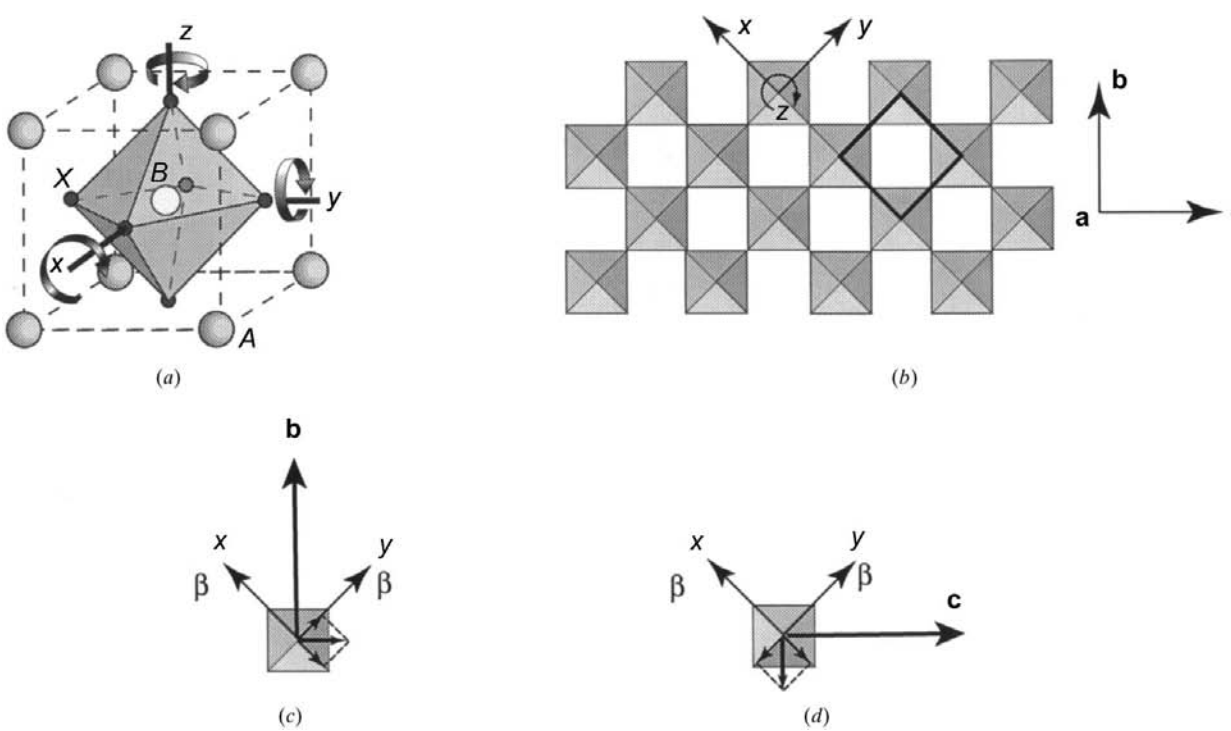

Fig. 3. (*a*) Rotation of a single octahedron about its three fourfold axes *x*, *y* and *z*. (*b*) Relation between the '*x*', '*y*' and 'z' fourfold axes of an octahedron and **a**, **b** and **c** axes of a {110} layer. (*c*) Sum of rotations of equal magnitude (β) about both '*x*' and '*y*' fourfold axes, equivalent to the rotation of a single octahedron about its twofold axis parallel to the **b** axis of a layer. (*d*) Sum of rotations of equal magnitude about both '*x*' and '*y*' fourfold axes, resulting in a tilt of an octahedron about its twofold axis parallel to the **c** axis of a layer. Vectors in both (*c*) and (*d*) indicate the direction of rotations about the corresponding axes. Note the difference in the sign of rotation about the '*x*' axis in (*c*) and (*d*).

Table 4. *Layer, G_3^2 and space G_3^3 group symmetry for $A_nB_nX_{3n+2}$ structures with $c = a_c2^{1/2}$*

The numbers in brackets for the layer group indicate the number of groups according to common classification (Schubnikov & Koptsik, 1974). The numbers in brackets for the space group indicate both the number of a group and axes setting, respectively, according to Table 4.3.1 of the *International Tables for Crystallography* (1995, Vol. A).

Layer tilt system number	Tilt for a layer	Motif {**e**}, [01] type			Motif {**o**}, [00] type			Comments
		G_3^2	G_3^3, **O**	G_3^3, **M**	G_3^2	G_3^3, **O**	G_3^3, **M**	
27	$\alpha^0\beta^0\beta^0$	*pmcm* (43)	*Cmcm* (63,1)	None	*pmmm* (23)	*Immm* (71,1)	None	**a** = a_p
25	$\alpha^-\beta^0\beta^0$	*pmca* (46)	*Pbca* (61,1)	*P*11*a* (7,3)	*pmaa* (41)	*Pnaa* (56,4)	$P112_1$ (4,3)	
26	$\alpha^0\beta^-\beta^0$	*P*2/*m*11	*P*2/*b*11 (13,6)	*P*1 (1)	$p2_1/m11$ (18)	$p2_1/n11$ (14,6)	*P*1 or *P*11*b*	
23	$\alpha^+\beta^0\beta^0$	$pmc2_1$ (30)	$Cmc2_1$ (36,1)	None	*p*2/*m*11 (17)	*Pmnn* (58,4)	None	**a** = a_p
22	$\alpha^0\beta^-\beta^-$	*pmna* (44)	*Pbna* (60,5)	$P112_1/a$ (14,3)	*pmma* (25)	*Pnma* (62,1)	*A*112/*a* (15,3)	**b** tilt
		pmcm (43)	*Pbcm* (57,1)	$P112_1/m$ (11,3)	*pmam* (43)	*Pnam* (62,6)	*A*112/*m* (12,3)	**c** tilt
21	$\alpha^-\beta^0\beta^-$	*p*1 (1)	*P*1 (1)	*P*1 (1)	*p*1 (1)	*P*1 (1)	*P*1 (1)	
20	$\alpha^0\beta^-\gamma^-$	*P*2/*m*11 (17)	*P*2/*b*11 (14,6)	*P*1 (1)	$p2_1/m11$ (18)	$p2_1/n11$ (14,6)	*P*1 (1)	
17	$\alpha^+\beta^0\gamma^-$	*pm*11 (17)	*Pb*11 (7,5)	*P*1 (1)	$p2_1/m11$ (18)	$P2_111$ (4,6)	*P*1	
8	$\alpha^+\beta^-\gamma^-$	*pm*11	*Pb*11 (7,5)	*P*1	$p2_1/m11$ (18)	$P2_111$ (4,6)	*P*1	
12	$\alpha^-\beta^-\beta^-$	*p*11*a* (10)	$P112_1/a$ (14,3)	$P112_1/a$ (14,3)	*P*112/*a*	*P*112/*a* (13,3)	*P*112/*a* (13,3)	$\mathbf{a}^-\mathbf{b}$ tilt
		*p*12/*c*1 (20)	*P*12/*c*1 (13,1)	*P*1	*P*12/*a*1	*P*1*a*1 (7,1)	*P*1	$\mathbf{a}^-\mathbf{c}$ tilt
11	$\alpha^-\beta^-\gamma^-$	*p*1	*P*1	*P*1	*p*1	*P*1	*P*1	
10	$\alpha^+\beta^-\beta^-$	$pmn2_1$ (35)	$Pbn2_1$ (33,2)	$P112_1$ (4,3)	$p2_1/m11$	$P2_12_12_1$ (19,1)	$P112_1/b$ (14,3)	$\mathbf{a}^+\mathbf{b}$ tilt
		$pmc2_1$ (30)	$Pbc2_1$ (29,2)	$P112_1$	$p2_1/m11$	$P2_12_12_1$	$P112_1/b$	$\mathbf{a}^+\mathbf{c}$ tilt

Table 5. *Space-group symmetry for the structures with a fractional value of n*

Layer tilt system number	Tilt for slab	G_3^2		G_3^3, motif {**eo**}, type [0$\underline{0}$]		G_3^3, motif {**eooe**}, type [0$\underline{1}$]		Comments
		e layer	**o** layer	**O**	**M**	**O**	**M**	
27	$\alpha^0\beta^0\beta^0$	*pmcm*	*pmmm*	*Ammm* (64,3)	None	*Pmnm*	None	**a** $\simeq a_p$
25	$\alpha^-\beta^0\beta^0$	*pmca*	*pmaa*	*I*2*cb* (45,3)	*P*11*a*	*P*11*a* (7,4)	*P*11*a*	
26	$\alpha^0\beta^0\beta^-$	*pm*11	$p2_1/m11$	$P2_111$ (4,5)	*P*1	*P*1 (1)	*P*1	
23	$\alpha^+\beta^0\beta^0$	$pmc2_1$	*p*2/*m*11	*Pmcb* (55,3)	None	$Pmn2_1$ (31,1)	None	$\mathbf{a}^+$ tilt, $a \simeq a_p$
22	$\alpha^0\beta^-\beta^-$	*pmna*	*pmma*	*I*2*mb* (46,3)	*P*11*a*	*P*112/*a* (13,3)	*P*112/*a*	**b** tilt
		pmcm	*pmam*	*I*2*cm* (46,4)	*P*11*m*	$P112_1/m$ (11,4)	$P112_1/m$	**c** tilt
21	$\alpha^-\beta^0\beta^-$	*p*1	*p*1	*P*1 (1)	*P*1	*P*1	*P*1	
20	$\alpha^0\beta^-\gamma^-$	*pm*11	$p2_1/m11$	$P2_111$ (4,5)	*P*1	*P*1	*P*1	
17	$\alpha^+\beta^0\gamma^-$	*pm*11	$p2_1/m11$	*P*1 (1)	*P*1	*p*1	*P*1	
8	$\alpha^+\beta^-\gamma^-$	*pm*11	$p2_1/m11$	$P2_111$ (4,5)	*P*1	*P*1	*P*1	
11	$\alpha^-\beta^-\gamma^-$	*p*1	*p*1	*P*1 (1)	*P*1	*P*1	*P*1	
12	$\alpha^-\beta^-\beta^-$	*p*11*a*	*p*112/*a*	*P*112/*a* (13,4)	*p*112/*a*	*P*11*a* (7,4)	*P*11*a*	$\mathbf{a}^-\mathbf{b}$ tilt
		*p*12/*c*1	*p*12/*a*1	*P*1*a*1 or *P*1*c*1 (7,2)	*P*1	*P*1	*P*1	$\mathbf{a}^-\mathbf{c}$ tilt
10	$\alpha^+\beta^-\beta^-$	$pmn2_1$	$p2_1/m11$	$P2_1nb$ (33,3)	$P112_1/b$	$P112_1$	$P112_1/b$	$\mathbf{a}^+\mathbf{b}$ tilt
		$pmc2_1$	$p2_1/m11$	$P2_1cn$ (33,4)	$P112_1/b$	$P112_1$	$P112_1/b$	$\mathbf{a}^+\mathbf{c}$ tilt

3.2. *Symmetry of {110}-type layers as diperiodic groups*

Layers are three-dimensional objects with two-dimensional translational symmetry, and therefore their symmetries are described by the 80 diperiodic (layer) G_3^2 groups. A detailed description and classification of the layer groups can be found in a monograph by Schubnikov & Koptsik (1974). A number of limitations on the symmetry elements of these groups are imposed by the absence of translational symmetry in the third dimension (normal to a layer plane): only twofold axes are allowed in the layer plane, and translations of both screw axes and glide planes must be parallel to this plane. In the case of the $\{110\}_c$-type layers, the symmetry depends on both the layer type ('**e**' or '**o**') and on the tilt system.

The symmetry of an individual '**e**' or '**o**' layer is determined from projection of the layer structure along the **a** direction. A tilt of the projected octahedron is indicated in the drawings by a graphical code (Fig. 4). Doubling of the periodicity along the projection axis from an $\mathbf{a}^-$ tilt, or from any tilt about the out-of-plane pseudo-fourfold axes of an octahedron, was taken into account. The symmetry elements of a layer group were established from the distribution of coded octahedra.

Fig. 4 is an example of an $\alpha^+\beta^-\beta^-$ tilt system which applies to both '**e**' and '**o**' layers. This tilt system can be considered as a superposition of $\mathbf{a}^+$ and **b** tilts. The '**e**' layer contains a diagonal n_y glide (subscript '*y*' indicates that the plane is normal to the **b** axis), a mirror m_x and the 2_{1z} screw axis (*z* indicates that this axis is parallel to the **c** axis; Fig. 4*a*). Accordingly, the symmetry of this

layer is fully described by the diperiodic group $pmn2_1$. For the '**o**' layer, Fig. 4(*b*), there are only two symmetry elements, 2_{1x} and m_x, corresponding to the diperiodic group $p2_1/m11$. Layer G_3^2 groups for all 12 tilt systems of interest were determined for '**o**' and '**e**' layers and are listed in Tables 4 and 5. The symbols of the layer groups correspond to the setting of axes with the **b** axis normal to the layers.

3.3. *Effect of octahedral tilting on a Bravais lattice*

For the layers assembled in a periodic structure, the type of Bravais lattice depends on both the layer stacking sequence within a motif and on the sense of a tilt (tilt phases) in different layers. Here, we consider the possible Bravais lattices only for the most symmetrical layers with $\mathbf{a}^+$, **b** and **c** tilts around the corresponding orthorhombic axes.

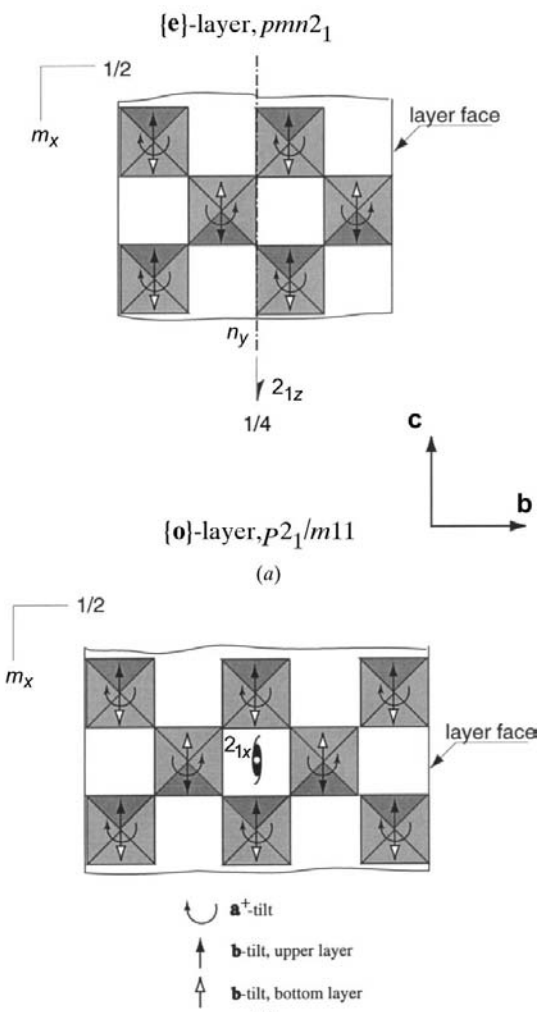

Fig. 4. Schematic projections along **a** direction of both {**e**} (*a*) and {**o**} (*b*) layers with $\mathbf{a}^+\mathbf{b}$ tilt. The symmetry elements of the layers are superimposed.

For an $\mathbf{a}^+$ tilt, the relationships between the sense of a tilt for octahedra on opposite sides of a spacer must be considered. There are two possible cases: octahedral tilts on the faces of neighboring layers are either in-phase (*a*) or anti-phase (*b*), as depicted in Figs. 5(*a*) and (*b*). The anti-phase configuration (Fig. 5*b*) yields a more uniform distribution of bonds in the spacer, and is therefore associated with much lower energy structures than the in-phase configuration. We therefore consider only the anti-phase tilt relation in the following treatment. It is easy to show that for the [01]-type motif, the **C**-centered lattice of the untilted structure is preserved. However, for both [00]- and [0$\underline{0}$]- motifs there is a change in orthorhombic centering from **I** and **A** to **P**.

Both the **b** and the **c** tilt lead to doubling of the *a* lattice parameter (see Figs. 5*c* and *d*). In this case, the Bravais lattice is also determined by the tilt phases of octahedra which were related by the **b** lattice translation in the untilted orthorhombic structure. The effect of the **b** tilt on the Bravais lattices of $A_nB_nX_{3n+2}$ structures has been described by Nanot *et al.* (1981), but the present analysis provides a more complete classification by including compound motifs. In the compound motifs, the phases of tilts across a spacer must be considered. For

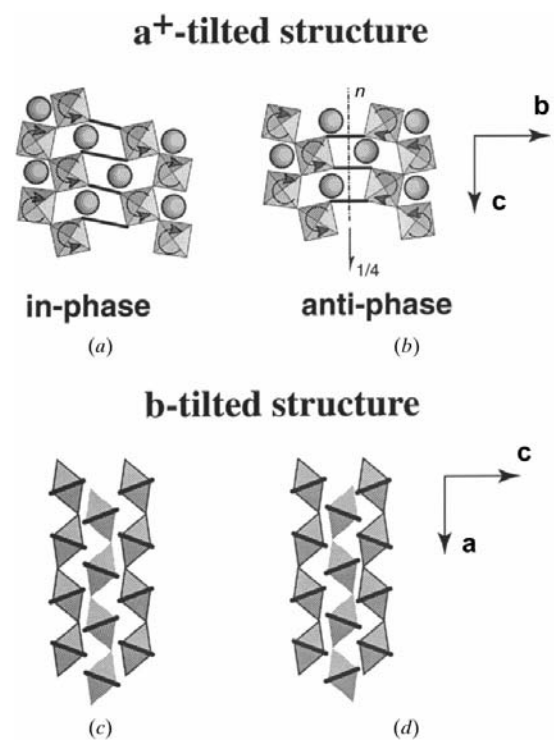

Fig. 5. Structure of a spacer for both in-phase (*a* and *c*) and anti-phase (*b* and *d*) tilts of octahedra at the layer faces on both sides of a spacer. Note the difference in the structure of a spacer in (*a*) and (*b*), corresponding to the $\mathbf{a}^+$ tilt. Some of the $X-X$ bonds across the spacer are indicated. For the **b** tilt, both in-phase (*c*) and anti-phase (*d*) tilt relations result in the same structure of a spacer.

the **b** and the **c** tilt, there is no difference in the structure of a spacer for both the in-phase (Fig. 5*a*) or the anti-phase (Fig. 5*b*) tilt relations.

The effects of **b** (**c**) tilt phase relations on a Bravais lattice were analyzed for different types of motifs (see *Appendix B*). For [00], [01] and [0$\underline{0}$] motifs, which have the same sense of tilt for octahedra related by the **b** lattice translation of the untilted structure, the orthorhombic **I**-, **C**- and **A**-centered lattices change to a primitive (**P**) orthorhombic lattice with $a' = 2a$. In these structures, the change in tilt phase in a second motif results in the *same*, but *mirror*-reflected, lattice (or in a twin structure). Different relations in the tilt phase within a compound motif *do not* change the lattice. If the octahedra, related by the **b** lattice translation in an untilted structure, are tilted in *anti-phase*, an orthorhombic lattice changes to a monoclinic lattice (**c** is the unique axis) as follows:

[00] type: **I**-centered (oI) → **A**-centered monoclinic (mA) or oI → **I**-centered monoclinic (mI);

[01] type: $oC \rightarrow mP$;

[0$\underline{0}$] type: $oA \rightarrow mP$;

[0$\underline{1}$] type: $oP \rightarrow mP$.

In structures with a combination of tilts, *e.g.* $\mathbf{a}^+\mathbf{b}$ or $\mathbf{a}^+\mathbf{c}$, the lattice will have the lowest symmetry and smallest lattice translations.

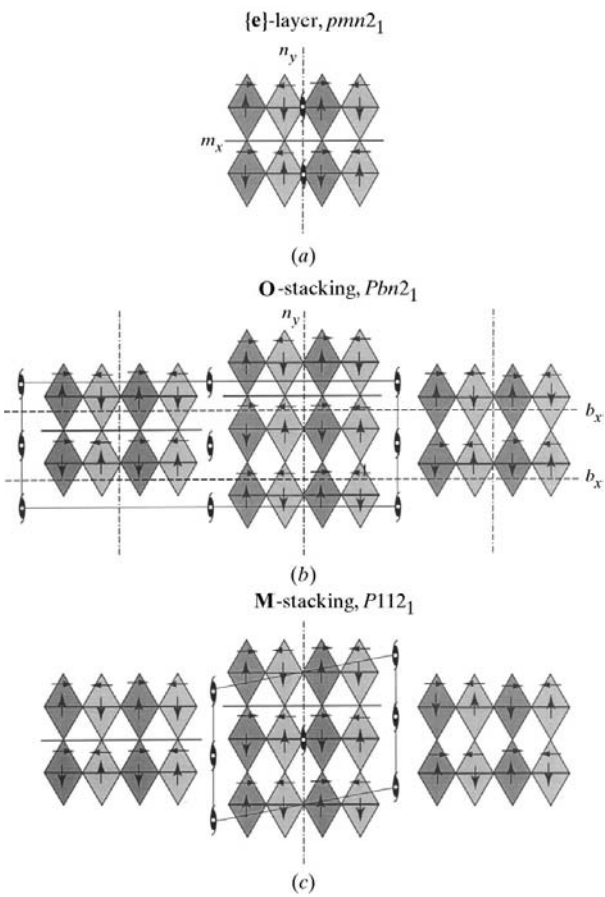

Fig. 6. (*a*) [001] schematic projections of the {**e**} layer with $\mathbf{a}^+\mathbf{b}$ tilt and the structures resulting from the translation of this layer with both **O** and **M** phase relations. The symmetry elements are superimposed. (*b*) Both n_y and 2_{1z} symmetry elements of the layer are preserved, while the mirror m_x does not apply to the whole structure. The combination of m_x with a translation of the layer generates a b_x glide, and the combination of both n_y and b_x results in the 2_{1z} axes located in the spacer. Such a set of symmetry elements corresponds to the $Pbn2_1$ space group. (*c*) The space group of the **M**-type structure is the subgroup of the space group for the **O** structure with 2_{1z} axes only preserved. The resulting space group is $P112_1$ (**c** is the unique axis).

3.4. *Space groups of the tilted $A_nB_nX_{3n+2}$ structures*

In the following discussion, we will use symbols '**O**' and '**M**' to distinguish the structures in which **b** and **c** tilt phases (in different layers) result in the orthorhombic (oC, oI, oA, oP) or monoclinic lattices (mP, mI, mA), respectively.

The space groups of the $A_nB_nX_{3n+2}$ structures were derived from the layer groups by combining (i) the symmetry elements of a layer group (see §3.2) which survived the translation of stacking, and (ii) symmetry elements that are generated by the translation for the particular stacking arrangement. Typically, it was sufficient to establish the presence of any of these additional symmetry operations to deduce the space group of the resulting structure from the combinations of symmetry elements. The derivation was conducted for both the **O** and the **M** structures composed of all four types of motifs, namely [01]-{**e**}, [00]-{**o**}, [0$\underline{0}$]-{**eo**} and [0$\underline{1}$]-{**eooe**}. Space groups of the possible structures are enumerated in Tables 4 and 5.

Examples of a structure composed of {**e**} layers with $\mathbf{a}^+\mathbf{b}$ tilt are analyzed in Fig. 6. In this case, both n_y and 2_{1z} symmetry elements of an isolated layer are preserved for **O** stacking, while the m_x of the layer *does not* apply to the whole structure (Fig. 6). The **O** stacking of **e** layers generates b_x glides which relate the octahedra in adjacent layers. Such a combination of symmetry elements corresponds to space group $Pbn2_1$. The space group for the **M** arrangement of **e** layers is $P112_1$ (mP lattice + 2_{1z} symmetry axis preserved by **M** stacking).

4. Maximal group/subgroup relationship approach

The space group of a tilted structure can also be derived as a subgroup (not necessarily maximal) of an untilted aristotype structure by identifying (i) the symmetry elements that are lost due to an operation of a particular tilt and (ii) the phase relationship between tilts in different layers. The resulting subgroup can be determined with the help of the *International Tables for Crystallography* (1995, Vol. A). We confine our group/subgroup analysis only to the simplest motifs ({**e**}, {**o**}, {**eo**}), the most symmetrical tilt systems ($\mathbf{a}^+$, **b**, **c** tilts) and phase relations (**O**, **M**). The space groups of the untilted

structures with {**e**}, {**o**} and {**eo**} motifs were determined in §2.3 as *Cmcm*, *Immm* and *Ammm*, respectively.

Fig. 7 shows an example of changes in symmetry due to octahedral tilting. This schematic drawings represents the $n = 4$ untilted and tilted structures, with $\mathbf{a}^+$, **b** and **c** tilts, and **O**-type stacking, as projected along [100]. The symmetry elements of these structures were identified and superimposed onto the projections. The sets of the symmetry elements and Bravais lattices of these structures lead to space groups $Cmc2_1$, *Pbcn* and *Pbcm* for the structures with pure $\mathbf{a}^+$, **b** and **c** tilts, respectively. Using these diagrams, the removal of symmetry elements resulting from different tilt systems can be deduced. From changes in the Bravais lattice plus the reduction of symmetry elements, the maximal symmetry group/subgroup relations can be established. Fig. 8 shows an example of the subgroup tree for the structure with {**e**} motif, where decreases in symmetry are indicated by the descending arrows. The tree describes symmetry reductions resulting from the $\mathbf{a}^+$, **b** and **c** tilts, and various tilt combinations. Note that the space groups of structures with combined tilts (*e.g.* $\mathbf{a}^+\mathbf{b}$ and $\mathbf{ba}^+$) are independent of the order of the tilts. Subgroup trees for both the {**o**} and the {**eo**} motif are given in *Appendices C* and *D*. Comparison of space groups obtained by the group/subgroup procedure with those obtained by the stacking of layers (Tables 4 and 5) shows that they are identical.

5. Comparison of symmetry analysis and experimental data on $A_nB_nX_{3n+2}$ structures

All space groups derived in the present analysis exactly match those determined experimentally for the corresponding motifs. Moreover, the approximations of octahedral distortions in the experimentally determined structures by $\mathbf{a}^+$-, **b**- and **c**-type tilts fit the tilt systems from our analysis (compare Table 1 with Tables 4 and 5). Experimentally determined structures often show an appreciable distortion of tilted octahedra, which are accompanied by the displacements of the *A* and *B* cations away from ideal positions. Nevertheless, in most of the $A_nB_nX_{3n+2}$ compounds observed these displacements are compatible with the symmetry imposed by the pure tilting of *rigid* octahedra.

Comparison of our symmetry analysis (Tables 4 and 5) with the experimentally determined space groups (Table 1) suggests that the symmetries of most of the room-temperature compounds correspond to a combination of both $\mathbf{a}^+$ and **b** tilts. Three structures with pure **c** tilts have been reported in the literature. The compound $BaMnF_4$ exhibits a combination of $\mathbf{a}^+$ and **c** tilts, with the **c** tilt resulting in an incommensurate modulation. A single compound, $NaCrF_4$, with a combination of both $\mathbf{a}^-$ and **b** tilts, has been identified. No structures with purely either **b** or $\mathbf{a}^-$ tilting, nor with a doubled **c** periodicity, have been reported. Space groups of the observed compounds permit structures which in our classification correspond to the motifs {**e**}, {**o**} and {**eo**} ([01], [00] and [0$\underline{0}$] types), and both **O** and **M** tilt phase relations. The atomic positions determined by the refinement of single-crystal X-ray diffraction data suggest that the orthorhombic symmetry of a layer can be preserved even in structures having monoclinic lattices (due to the **M** tilt phase relation; Gasperin, 1975; Koz'min *et al.*, 1997). So far, this observation is general and holds for all known $A_nB_nX_{3n+2}$ compounds.

Recent ground-state energy calculations performed for various tilt systems in simple perovskites suggested that an orthorhombic $a^+b^-b^-$ tilt (equivalent to the combinations of tilts $\mathbf{a}^+\mathbf{b}$ and $\mathbf{a}^+\mathbf{c}$ in this work) results in the most stable structure for the compounds with tolerance factors $t < 0.975$ (Woodward, 1997*b*). The present analysis shows that the $\mathbf{a}^+\mathbf{b}$ tilt system, and not $\mathbf{a}^+\mathbf{c}$, occurs in many $A_nB_nX_{3n+2}$ compounds, although the energy calculations for these layered structures have yet to be performed. As compared to a simple perovskite, the energetic balance for $A_nB_nX_{3n+2}$ structures is

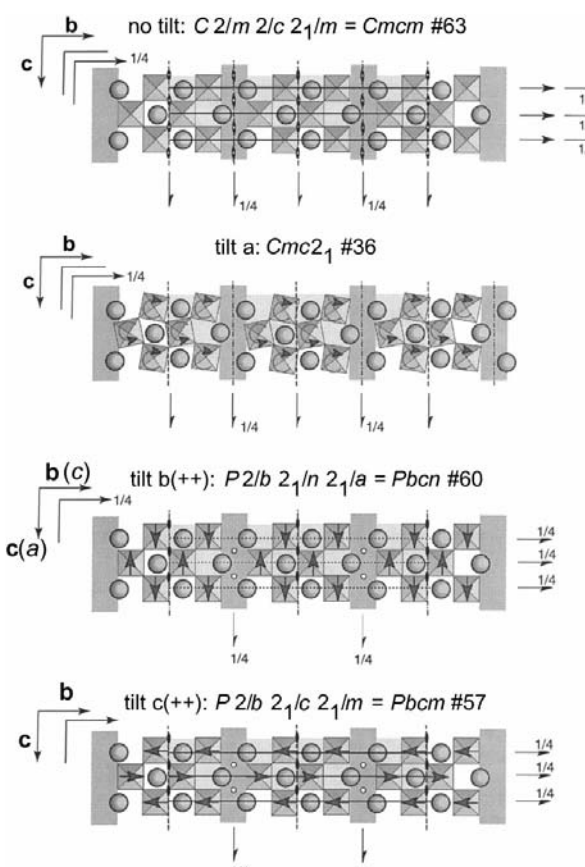

Fig. 7. [100] schematic projections of the structures composed of {**e**} layers with the symmetry elements superimposed. (*a*) Untilted structure, space group *Cmcm*. (*b*) $\mathbf{a}^+$ tilt, space group $Cmc2_1$. (*c*) **b** tilt, space group *Pbcn*. (*d*) **c** tilt, space group *Pbcm*.

complicated by the interlayer region (spacer) between the layers, which results in abnormal coordination of A ions adjacent to the spacer. The distribution of $A-X$ bonds in the spacer apparently can make a significant contribution to the stabilization of a specific structure.

The sequences of symmetry maximal group/subgroup relationships represent possible paths for phase transitions determined by the tilting of octahedra. The application of our symmetry analysis to the experimental results on phase transitions in $A_nB_nO_{3n+2}$ compounds suggests that in most cases the displacive transition from a high-temperature untilted structure to a low-temperature tilted structure occurs in two stages: untilted $\rightarrow$ $\mathbf{a}^+ \rightarrow \mathbf{a}^+\mathbf{b}$, with doubling of the a lattice parameter. The group/subgroup relationship between the initial and final structures for the second transition is not maximal, but the intermediate structure (which represents a formal transition state of the transformation) has never been observed. No system with the sequence of transitions untilted $\rightarrow$ $\mathbf{b} \rightarrow \mathbf{a}^+\mathbf{b}$ has been reported.

In some systems, the $\mathbf{a}^+ \rightarrow \mathbf{a}^+\mathbf{b}$ transition results in a one-dimensionally modulated incommensurate structure, with a modulation having a periodicity close to $2\mathbf{a}$ ($\mathbf{a}$ is the periodicity of the $\mathbf{a}^+$-tilted structure; Yamamoto *et al.*, 1980; Nanot *et al.*, 1986). The modulation wave has been attributed to the alternating tilting of BX_6 octahedra around the **b** axis. The three-dimensional space group describes an approximation for the corresponding incommensurate structure with a phase of modulation locked in. Experimental studies of such compounds are considered in a subsequent report (Levin *et al.*, 1999).

6. Conclusions

A classification scheme that relates the stacking sequences of $\{110\}_c$-type layers and octahedral tilt systems to the symmetry of $A_nB_nX_{3n+2}$ structures has been developed using two complimentary methods. In the first, the symmetry of a layer was identified with one of the 32 G_3^2 diperiodic (layer) groups for each of Glazer's 23 tilt systems in a perovskite. Then the G_3^3 space groups of the layered $A_nB_nX_{3n+2}$ structures were constructed by translating the layer (motif) according to the particular type of stacking arrangement. In the second method, the symmetries of tilted structures were derived from those of untilted structures by systematically applying different octahedral tilts and following maximal symmetry group/subgroup relations.

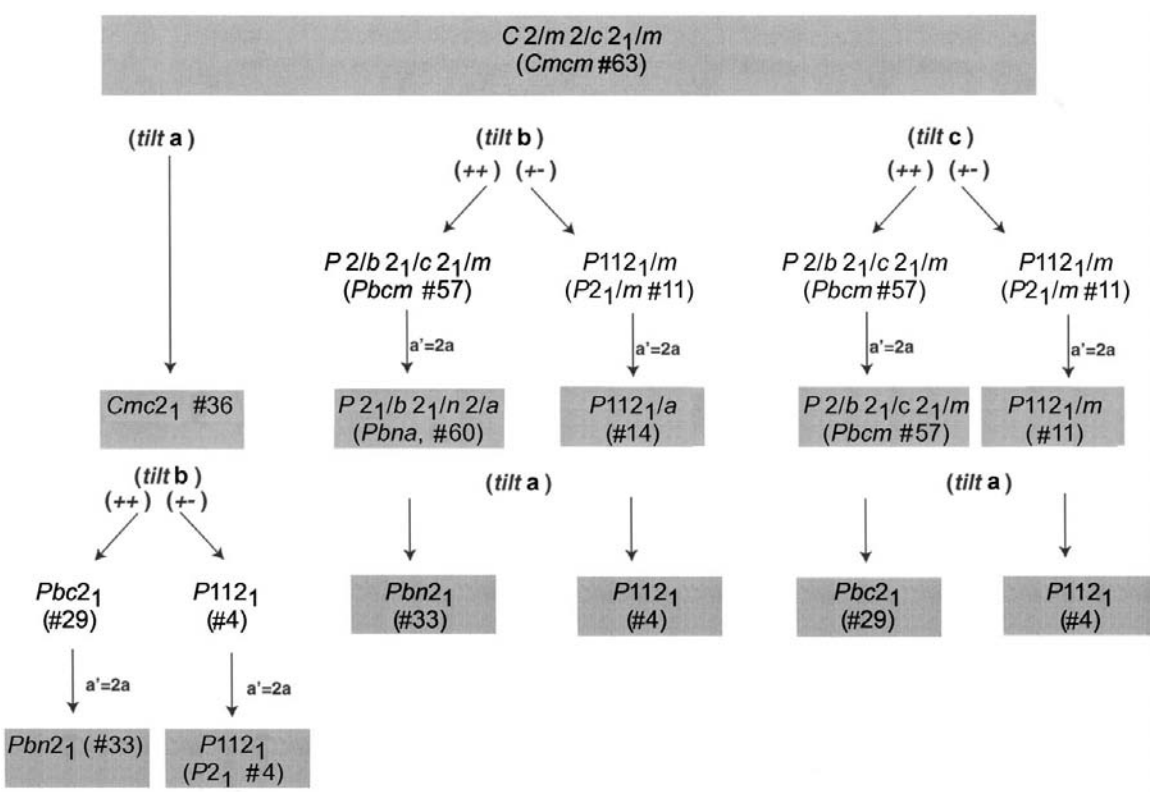

Fig. 8. Maximal symmetry group/subgroup tree for the structures composed of [01] motifs. The symmetry reductions corresponding to the $\mathbf{a}^+$, **b** and **c** tilts are indicated by the descending arrows. The numbers in brackets refer to the number of space group and the number of axes setting according to Table 4.3.1 of the *International Tables for Crystallography* (1995, Vol. A).

The general derivation of the ten space groups for untilted structures covers all possible layer stackings. From these aristotype structures, the space groups of tilted structures can be deduced by group/subgroup analysis. Such analysis was performed for a limited number of motifs ({**e**}, {**o**} and {**eo**}) and for the most symmetrical tilt systems (**a**$^+$, **b** and **c** tilts). General analysis of the symmetries of the {110} layers for all possible tilt systems was performed, and the space groups for the {**e**}, {**o**}, {**eo**} and {**eooe**} motifs were derived. Comparison of the symmetry analysis with experimental data demonstrates that the symmetries of most of the $A_nB_nX_{3n+2}$ structures are fully determined by octahedral tilt systems for rigid BX_6 octahedra. In the most symmetrical tilt systems, the octahedral tilting pattern can be uniquely deduced from space-group symmetry. Experimentally, the most commonly observed tilt system is a combination of tilts around both orthorhombic **a** and **b** axes. The symmetry relations between untilted and tilted structures were described by sequences of maximal group/subgroup relations for a number of the common tilt systems. The resulting symmetry trees, which relate untilted to tilted structures, are important for both the analysis of possible phase transitions and for predictions of microstructure.

APPENDIX *A*

Table 6 shows the 27 tilt systems possible in a {110} layer resulting from the 23 tilt systems possible in a three-dimensional perovskite structure according to the notation of Glazer (1972) (see §3.1).

APPENDIX *B*

Fig. 9 presents schematic illustrations of the effect of the **b** (or **c**) tilt on a Bravais Lattice for different motifs (see §3.3). The squares represent rows of octahedra at the opposite faces of a motif (viewed along the **c** direction), while the difference in shade refers to a different sign of the tilt. This analysis does not depend on the type (**b** or **c**) of tilt. For [00], [01] and [0$\underline{0}$] motifs, which have the same sense of tilt for octahedra related by the **b** lattice translation of the untilted structure, the orthorhombic **I**-, **C**- and **A**-centered lattices change to a primitive (**P**) orthorhombic lattice with $a' = 2a$. In these structures, the change in tilt phase in a second motif results in the *same*,

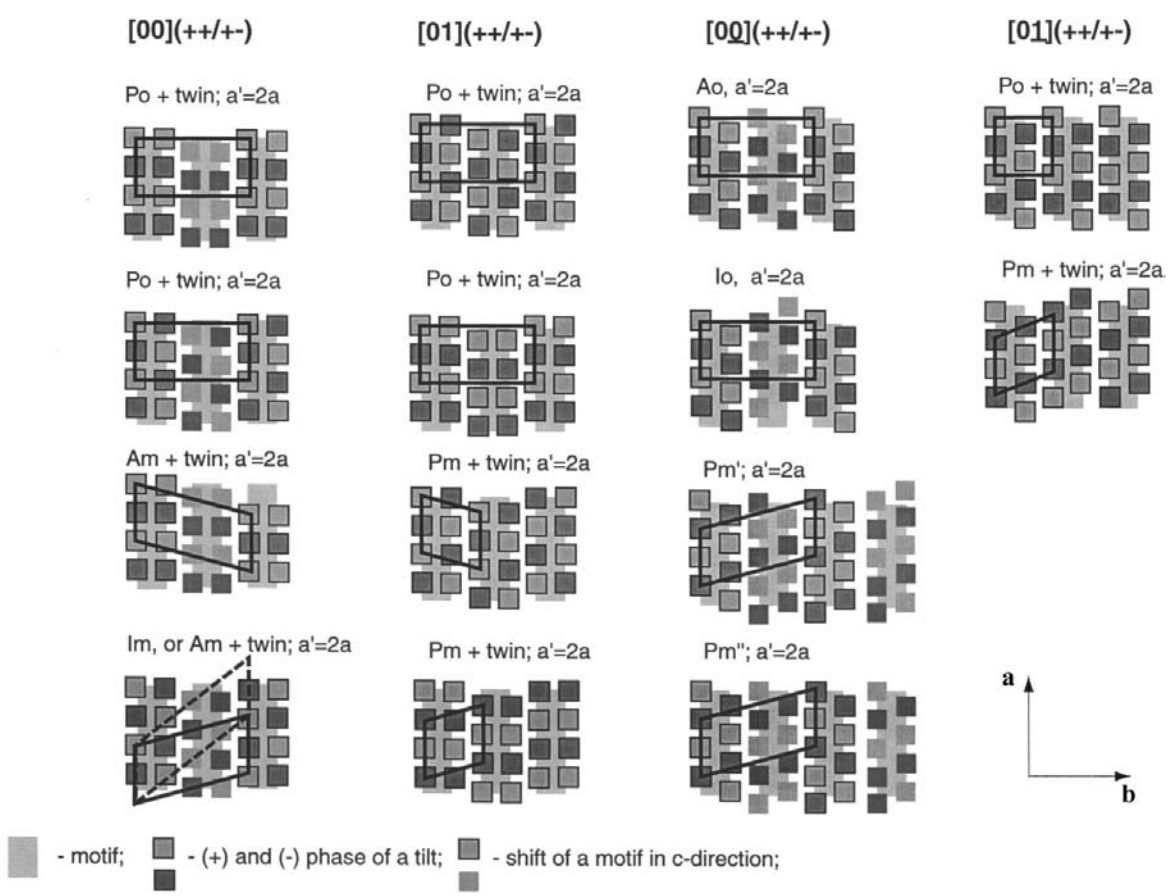

Fig. 9. Schemes of the effect of the **b** (or **c**) tilt on a Bravais lattice for different motifs.

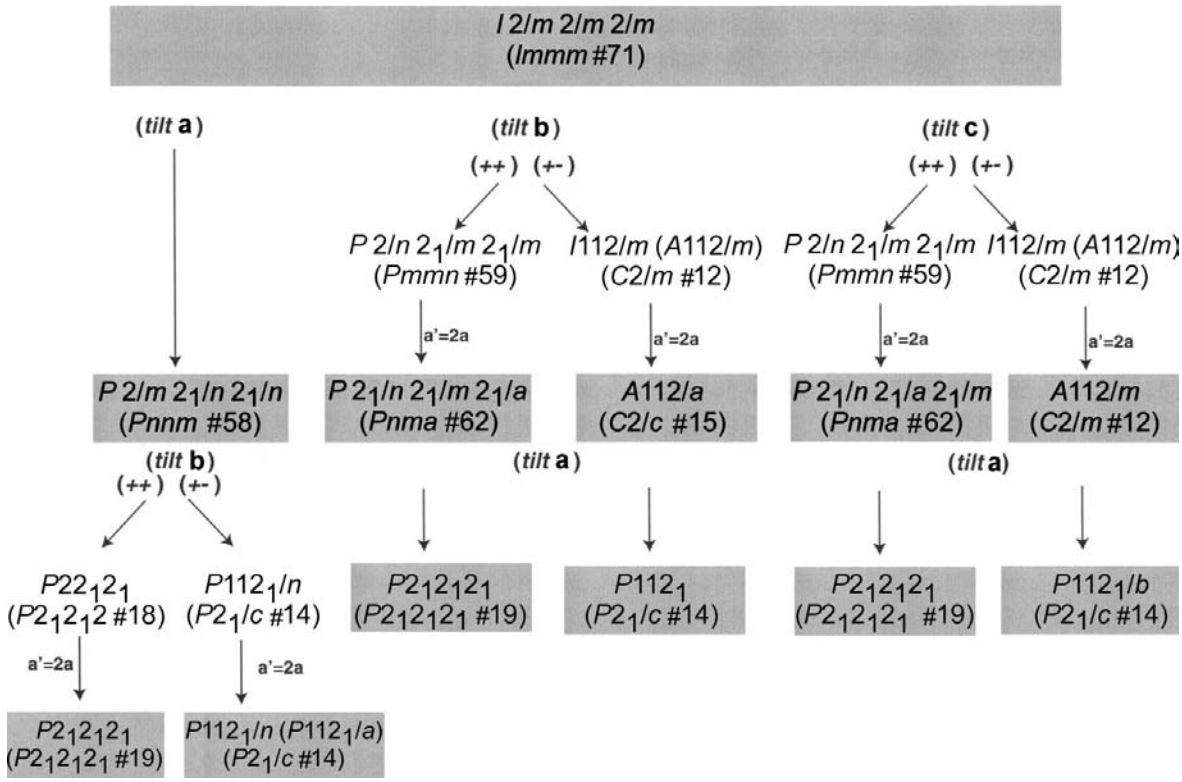

Fig. 10. Maximal symmetry group/subgroup tree for the structures composed of {**o**} motifs.

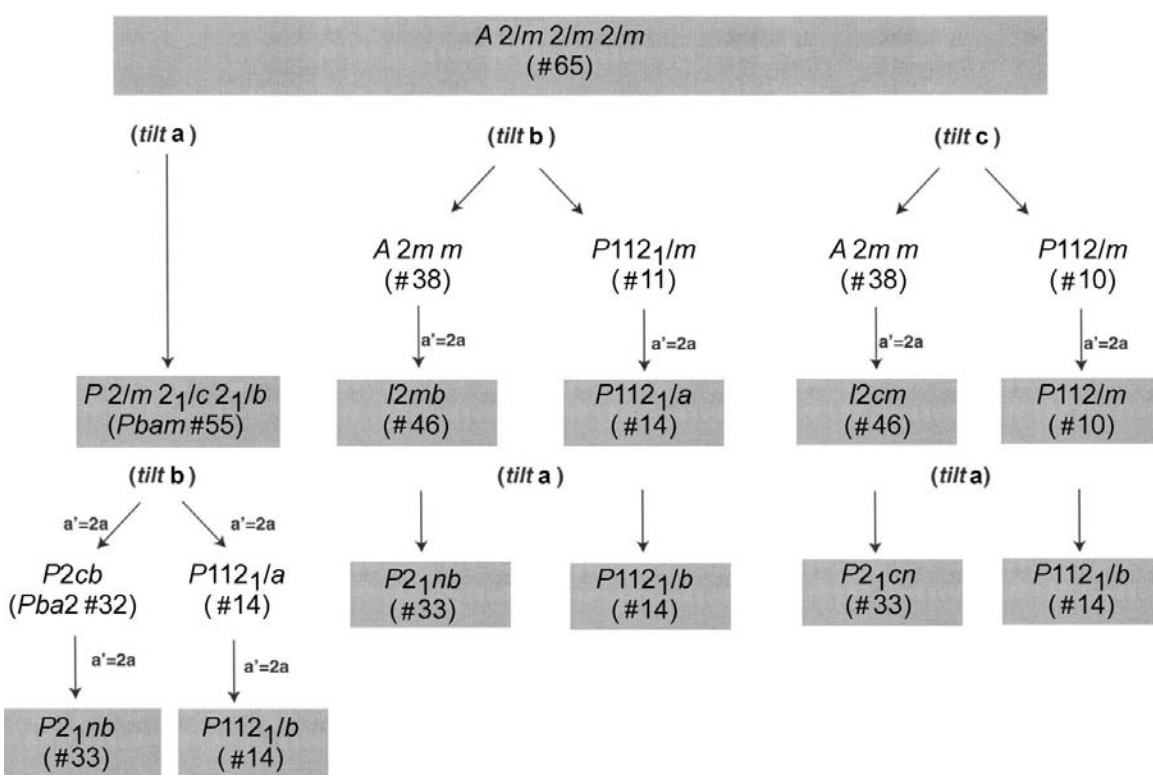

Fig. 11. Maximal symmetry group/subgroup tree for the structures composed of {**eo**} motifs.

Table 6. *Relation between the 23 tilt systems possible in a three-dimensional perovskite structure and the 27 tilt systems possible in a {110} layer*

Glazer's tilt system number	Glazer's tilt system	Tilt system number of the layer	Tilt system in a layer	Tilt about **a**, **b** and **c** axes
1	$\mathbf{a}^+\mathbf{b}^+\mathbf{c}^+$	1	$\alpha^+\beta^+\gamma^+$	
2	$\mathbf{a}^+\mathbf{b}^+\mathbf{b}^+$	2	$\alpha^+\beta^+\beta^+$	
3	$\mathbf{a}^+\mathbf{a}^+\mathbf{a}^+$			
4	$\mathbf{a}^+\mathbf{b}^+\mathbf{c}^-$	3	$\alpha^+\beta^+\gamma^-$	
		4	$\alpha^-\beta^+\gamma^+$	
5	$\mathbf{a}^+\mathbf{a}^+\mathbf{c}^-$	5	$\alpha^-\beta^+\beta^+$	
6	$\mathbf{a}^+\mathbf{b}^+\mathbf{b}^-$	6	$\alpha^+\beta^+\beta^-$	
7	$\mathbf{a}^+\mathbf{a}^+\mathbf{a}^-$			
8	$\mathbf{a}^-\mathbf{b}^+\mathbf{c}^-$	7	$\alpha^-\beta^+\gamma^-$	
9	$\mathbf{a}^+\mathbf{a}^-\mathbf{c}^-$	8	$\alpha^+\beta^-\gamma^-$	
		9	$\alpha^-\beta^+\beta^-$	
10	$\mathbf{a}^+\mathbf{b}^-\mathbf{b}^-$	10	$\alpha^+\beta^-\beta^-$	$\mathbf{a}^+\mathbf{b}$ or $\mathbf{a}^+\mathbf{c}$
11	$\mathbf{a}^+\mathbf{a}^-\mathbf{a}^-$			
12	$\mathbf{a}^-\mathbf{b}^-\mathbf{c}^-$	11	$\alpha^-\beta^-\gamma^-$	
13	$\mathbf{a}^-\mathbf{b}^-\mathbf{b}^-$	12	$\alpha^-\beta^-\beta^-$	$\mathbf{a}^-\mathbf{b}$ or $\mathbf{a}^-\mathbf{c}$
14	$\mathbf{a}^-\mathbf{a}^-\mathbf{a}^-$			
15	$\mathbf{a}^0\mathbf{b}^+\mathbf{c}^+$	13	$\alpha^0\beta^+\gamma^+$	
16	$\mathbf{a}^0\mathbf{b}^+\mathbf{b}^+$	14	$\alpha^+\beta^0\gamma^+$	
		15	$\alpha^0\beta^+\beta^+$	
17	$\mathbf{a}^0\mathbf{b}^+\mathbf{c}^-$	16	$\alpha^0\beta^+\gamma^-$	
		17	$\alpha^+\beta^0\gamma^-$	
		18	$\alpha^-\beta^0\gamma^+$	
18	$\mathbf{a}^0\mathbf{b}^+\mathbf{b}^-$	19	$\alpha^0\beta^+\beta^-$	
19	$\mathbf{a}^0\mathbf{b}^-\mathbf{c}^-$	20	$\alpha^0\beta^-\gamma^-$	
		21	$\alpha^-\beta^0\gamma^-$	
20	$\mathbf{a}^0\mathbf{b}^-\mathbf{b}^-$	22	$\alpha^0\beta^-\beta^-$	**b** or **c**
21	$\mathbf{a}^0\mathbf{a}^0\mathbf{c}^+$	23	$\alpha^+\beta^0\beta^0$	$\mathbf{a}^+$
		24	$\alpha^0\beta^0\beta^+$	
22	$\mathbf{a}^0\mathbf{a}^0\mathbf{c}^-$	25	$\alpha^-\beta^0\beta^0$	$\mathbf{a}^-$
		26	$\alpha^0\beta^-\beta^0$	
23	$\mathbf{a}^0\mathbf{a}^0\mathbf{a}^0$	27	$\alpha^0\beta^0\beta^0$	

but *mirror*-reflected, lattice (or in a twin structure). Different relations in the tilt phase within a compound motif can result in two types of motifs, [00]++ and [00]+−, but *do not* change the lattice.

APPENDIX *C*

Fig. 10 shows the maximal symmetry group/subgroup tree for the structures composed of {**o**} motifs (see §4).

APPENDIX *D*

Fig. 11 shows the maximal symmetry group/subgroup tree for the structures composed of {**eo**} motifs (see §4).

References

Alexandrov, K. S. (1976). *Ferroelectrics*, **14**, 801–805.

Alexandrov, K. S. & Bartolomé, J. (1994). *J. Phys. Condens. Matter*, **6**, 8219–8235.

Alexandrov, K. S. & Beznosikov, B. V. (1997). *Perovskite-Like Crystals*. Novosibirsk: Nauka. (In Russian.)

Alexandrov, K. S., Beznosikov, B. V. & Misyul, S. V. (1987). *Ferroelectrics*, **73**, 201–220.

Bednorz, J. G. (1997). *Physica C*, **282**, 37–40.

Brandon, J. K. & Megaw, H. D. (1970). *Philos. Mag.* **21**, 189–194.

Dance, J. M. (1981). *Mater. Res. Bull.* **16**, 599–606.

Deblieck, R., Van Tendeloo, G., Van Landuyt, J. & Amelinckx, S. (1985). *Acta Cryst.* B**41**, 319–329.

Di Domenico, M., Eibschutz, M., Guggenheim, H. J. & Camlibel, I. (1969). *Solid State Commun.* **7**, 1119–1125.

Drews, A. R., Wong-Ng, W., Roth, R. S. & Vanderah, T. A. (1996). *Mater. Res. Bull.* **31**, 153–160.

Gasperin, M. (1975). *Acta Cryst.* B**31**, 2129–2130.

Glazer, A. M. (1972). *Acta Cryst.* B**28**, 3384–3392.

Hatch, D. M. & Stokes, H. T. (1987). *Phys. Rev. B*, **35**, 8509–8516.

Howard, C. J. & Stokes, H. T. (1998). *Acta Cryst.* B**54**, 782–789.

Ishizawa, N., Marumo, F., Kimura, M. & Kawamura, T. (1975). *Acta Cryst.* B**31**, 1912–1915.

Isupov, V. A., Smirnova, E. P., Isupova, E. N., Zaitseva, N. V., Pikush, L. G. & Smolenskii, G. A. (1976). *Sov. Phys. Solid State*, **18**, 835–836.

Isupov, V. A., Smirnova, E. P., Isupova, E. N., Zaitseva, N. V., Shemenev, L. A., Pavlova, N. G., Chikanova, M. K. & Smolenskii, G. A. (1977). *Sov. Phys. Solid State*, **19**, 544–545.

Keve, E. T., Abrahams, S. C. & Bernstein, J. L. (1969). *J. Chem. Phys.* **51**, 4928–4936.

Keve, E. T., Abrahams, S. C. & Bernstein, J. L. (1970). *J. Chem. Phys.* **53**, 3279–3287.

Knoke, G., Verschaften, W. & Babel, D. (1979). *J. Chem. Res. (S)*, p. 213.

Koz'Min, P. A., Zakharov, N. A. & Surazhskaya, M. D. (1997). *Inorg. Mater.* **33**, 850–852.

Levin, I., Bendersky, L. A. & Vanderah, T. A. (1999). *Philos. Mag.* In the press.

Maguer, J. J., Corbion, G., Schriewer-Pottgen, M., Fompeyrine, J. & Darriet, J. (1995). *J. Solid State Chem.* **115**, 98–111.

Megaw, H. D. (1973). *Crystal Structures: a Working Approach.* Philadelphia: W. B. Saunders.

Nanamatsu, N. S., Kimura, M. & Kawamura, T. (1975). *J. Phys. Soc. Jpn*, **38**, 817–824.

Nanamatsu, S. & Kimura, M. (1974). *J. Phys. Soc. Jpn*, **36**, 1495.

Nanamatsu, S., Kimura, D. K., Matsushita, S. & Yamada, N. (1974). *Ferroelectrics*, **8**, 511–515.

Nanot, M., Queyroux, F. & Gilles, J.-C. (1979). *J. Solid-State Chem.* **28**, 137–147.

Nanot, M., Queyroux, F., Gilles, J.-C. & Capponi, J. J. (1986). *J. Solid-State Chem.* **61**, 315–323.

Nanot, M., Queyroux, F., Gilles, J.-C. & Portier, R. (1981). *J. Solid-State Chem.* **38**, 74–81.

Scheunemann, S. K. & Müller-Buschbaum, H. K. (1974). *J. Inorg. Nucl. Chem.* **36**, 1965–1972.

Scheunemann, S. K. & Müller-Buschbaum, H. K. (1975*a*). *J. Inorg. Nucl. Chem.* **37**, 1679–1680.

Scheunemann, S. K. & Muller-Buschbaum, H. K. (1975*b*). *J. Inorg. Nucl. Chem.* **37**, 1879–1881.

Schmalle, H. W., Williams, T., Reller, A., Lichtenberg, F., Widmer, D. & Bednorz, J. G. (1995). *Acta Cryst.* C**51**, 1243–1246.

Schnering, H. G. & Blekmann, P. (1968). *Naturwissenschaften*, **55**, 342–343.
Schubnikov, A. V. & Koptsik, V. A. (1974). *Symmetry in Science and Art.* New York: Plenum Press.
Sciau, P., Lapasset, J. & Grebille, D. (1988). *Acta Cryst.* B**44**, 108–116.
Sych, A. M. & Titov, Yu. A. (1981*a*). *Russ. J. Inorg. Chem.* **26**, 469–471.
Sych, A. M. & Titov, Yu. A. (1981*b*). *Russ. J. Inorg. Chem.* **26**, 1077–1079.
Tanaka, M., Sekii, H. & Ohi, K. (1985). *Jpn. J. Appl. Phys.* **24** (Suppl. 2), 814–816.
Wells, A. F. (1984). *Structural Inorganic Chemistry*. Oxford: Clarendon Press.
Weiden, M., Grauel, N. J., Horn, S. & Steglich, F. (1995). *J. Alloys Compd.* **218**, 13–16.
Williams, T., Lichtenberg, F., Widmer, D., Bednorz, G. & Reller, A. (1993). *J. Solid State Chem.* **103**, 375–386.
Woodward, P. M. (1997*a*). *Acta Cryst.* B**53**, 44–66.
Woodward, P. M. (1997*b*). *Acta Cryst.* B**53**, 32–43.
Yamamoto, N. (1982). *Acta Cryst.* A**38**, 780–789.
Yamamoto, N., Yagi, K., Honjo, G., Kimura, M. & Kawamura, T. (1980). *J. Phys. Soc. Jpn*, **48**, 185–191.